



HHS Public Access

Author manuscript

Adv Funct Mater. Author manuscript; available in PMC 2018 January 19.

Published in final edited form as:

Adv Funct Mater. 2017 January 19; 27(3): . doi:10.1002/adfm.201604213.

In Vivo Micro-CT Imaging of Human Mesenchymal Stem Cells Labeled with Gold-Poly-L-Lysine Nanocomplexes

Dr. Taeho Kim,

Russell H. Morgan Department of Radiology and Radiological Science, Division of MR Research, and Cellular Imaging Section and Vascular Biology Program, Institute for Cell Engineering, The Johns Hopkins University School of Medicine, 217 Traylor, 720 Rutland Ave, Baltimore, Maryland 21205, USA. Center for Nanoparticle Research, Institute for Basic Science (IBS), and School of Chemical and Biological Engineering, Seoul National University, Seoul 151-742, Korea

Dr. Nohyun Lee,

Russell H. Morgan Department of Radiology and Radiological Science, Division of MR Research, and Cellular Imaging Section and Vascular Biology Program, Institute for Cell Engineering, The Johns Hopkins University School of Medicine, 217 Traylor, 720 Rutland Ave, Baltimore, Maryland 21205, USA. Center for Nanoparticle Research, Institute for Basic Science (IBS), and School of Chemical and Biological Engineering, Seoul National University, Seoul 151-742, Korea

Dr. Dian R. Arifin,

Russell H. Morgan Department of Radiology and Radiological Science, Division of MR Research, and Cellular Imaging Section and Vascular Biology Program, Institute for Cell Engineering, The Johns Hopkins University School of Medicine, 217 Traylor, 720 Rutland Ave, Baltimore, Maryland 21205, USA

Irina Shats,

Russell H. Morgan Department of Radiology and Radiological Science, Division of MR Research, and Cellular Imaging Section and Vascular Biology Program, Institute for Cell Engineering, The Johns Hopkins University School of Medicine, 217 Traylor, 720 Rutland Ave, Baltimore, Maryland 21205, USA

Dr. Mirosław Janowski,

Russell H. Morgan Department of Radiology and Radiological Science, Division of MR Research, and Cellular Imaging Section and Vascular Biology Program, Institute for Cell Engineering, The Johns Hopkins University School of Medicine, 217 Traylor, 720 Rutland Ave, Baltimore, Maryland 21205, USA

Dr. Piotr Walczak,

Russell H. Morgan Department of Radiology and Radiological Science, Division of MR Research, and Cellular Imaging Section and Vascular Biology Program, Institute for Cell Engineering, The Johns Hopkins University School of Medicine, 217 Traylor, 720 Rutland Ave, Baltimore, Maryland 21205, USA

Prof. Taeghwan Hyeon, and

Correspondence to: Jeff W.M. Bulte.

Author Manuscript

Author Manuscript

Author Manuscript

Author Manuscript

Center for Nanoparticle Research, Institute for Basic Science (IBS), and School of Chemical and Biological Engineering, Seoul National University, Seoul 151-742, Korea

Prof. Jeff W.M. Bulte

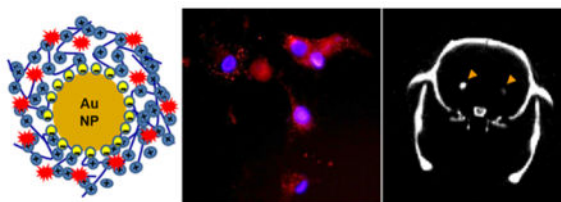
Russell H. Morgan Department of Radiology and Radiological Science, Division of MR Research, and Cellular Imaging Section and Vascular Biology Program, Institute for Cell Engineering, The Johns Hopkins University School of Medicine, 217 Traylor, 720 Rutland Ave, Baltimore, Maryland 21205, USA

Abstract

Developing *in vivo* cell tracking is an important prerequisite for further development of cell-based therapy. So far, few computed tomography (CT) cell tracking studies have been described due to its notoriously low sensitivity and lack of efficient labeling protocols. We present a simple method to render human mesenchymal stem cells (hMSCs) sufficiently radiopaque by complexing 40 nm citrate-stabilized gold nanoparticles (AuNPs) with poly-L-lysine (PLL) and rhodamine B isothiocyanate (RITC). AuNP-PLL-RITC labeling did not affect cellular viability, proliferation, or downstream cell differentiation into adipocytes and osteocytes. Labeled hMSCs could be clearly visualized *in vitro* and *in vivo* with a micro-CT scanner, with a detection limit of approximately 2×10^4 cells/ μ l *in vivo*. Calculated HU values were 2.27 /pg of intracellular Au as measured with inductively coupled plasma mass spectrophotometry (ICP-MS), and were linear over a wide range of cell concentrations. This linear CT attenuation was observed for both naked AuNPs and those that were taken up by hMSCs, indicating that the number of labeled cells can be quantified similar to the use of radioactive or fluorine tracers. This approach for CT cell tracking may find applications in CT image-guided interventions and fluoroscopic procedures commonly used for the injection of cellular therapeutics.

Graphical Abstract

AuNP-PLL-RITC nanocomplexes are used to label human mesenchymal stem cells in a simple and straightforward manner, allowing cells to be detected in a quantitative manner with an *in vivo* threshold of approximately 2×10^4 cells on micro-CT.



Keywords

Gold nanoparticles; cell tracking; molecular imaging; mesenchymal stem cell; computed tomography

1. Introduction

Stem cell therapy has received much attention in the field of regenerative medicine^[1] for the restoration of various tissues, including bone,^[2] cartilage,^[3] and the myocardium,^[4] as well as neurorepair.^[5] Adult human mesenchymal stem cells (hMSCs) are a particularly attractive cell source because they can be easily isolated, rapidly expanded *in vitro*, and successfully differentiated into multiple cell lineages.^[6]

A reliable means to noninvasively image the distribution of engrafted stem cells is pertinent to further develop the implementation of stem cell therapy. By tracking the location of transplanted cells serially in real time, the best dose and route of administration can be chosen dependent on the desired cell distribution. It can also be applied to determine the safety and efficacy of cell therapy, and aid in providing a go or no-go decision for further translation into clinical trials.^[7, 8] Various whole body imaging modalities can be used to track cells *in vivo*. These include positron-emission tomography (PET),^[9] single-photon emission tomography (SPECT),^[10] magnetic resonance imaging (MRI),^[11] magnetic particle imaging (MPI),^[12, 13] and ultrasound imaging (US).^[14] Clinically, computed tomography (CT) imaging is one of the more widely used imaging techniques due to its cost effectiveness, high-spatial resolution, short scan time, and ease of imaging procedure.^[15] However, very few CT cell tracking studies have been performed due to its low sensitivity and limited soft tissue image contrast as compared to magnetic resonance imaging.^[16]

To overcome the low sensitivity of CT contrast agents, bismuth,^[17] ytterbium,^[18] tungsten,^[19] tantalum,^[20] metal-organic framework,^[21] and gold nanoparticles have recently been developed to achieve a higher payload. Gold nanoparticles (AuNPs) are of particular interest because of its high elemental atomic number and efficient X-ray attenuation properties.^[22] Gold has a higher X-ray absorption coefficient than the clinical CT contrast agent element iodine (5.16 vs. 1.94 cm²/g at 100 keV, respectively), thus providing superior contrast.^[23] Many protocols exist for colloidal synthesis of AuNPs, and their size can be well controlled.^[24] Depending on their size and aggregation state, AuNPs are bioinert and exhibit low cytotoxicity when internalized into cells.^[25] For these reasons, they have been previously employed to track cells by CT, i.e., to detect *in situ* labeled macrophages in atherosclerotic plaques^[26] and encapsulated pancreatic islet cells transplanted in the peritoneum.^[27] However, these two scenarios used large entities (macrophages and microcapsules) as a facile means to achieve a high degree of AuNP incorporation. Improved labeling techniques are needed to enable a sufficient amount of labeling in smaller and/or non-phagocytic cells. Recently, it was shown that capping gold nanoparticles with 11-mercaptoundecanoic acid can greatly improve gold particle uptake in primary monocytes, allowing CT tracking of their migration in atherosclerotic plaques.^[28] Similarly, glucose capping can increase particle uptake in T cells for CT monitoring of cancer immunotherapy.^[29] In the present study, we aimed to develop a simple and straightforward, universally applicable method of labeling hMSCs with AuNPs to enable their *in vivo* visualization by micro-CT imaging.

2. Results and Discussion

2.1 Characterization of AuNP-PLL(RITC) Complexes

Citrate-stabilized AuNPs have a negative surface charge, which results in repulsion of the nanoparticles by the cell membrane.^[30] In order to achieve intracellular labeling, we complexed the particles with PLL as a cationic transfection agent. This macromolecule has previously been applied to efficiently label mammalian cells with superparamagnetic iron oxide (SPIO) nanoparticles for magnetic resonance^[31, 32] and magnetic particle^[12] imaging. In order to make labeled cells visible with fluorescence microscopy, we covalently bound RITC to PLL using the amine and isothiocyanate groups of PLL and RITC, respectively (Figure 1a).^[33] We then determined the average size and the electrophoretic (zeta) potential of naked AuNP and AuNP-PLL-RITC nanocomplexes. Upon PLL complexation, we found the smaller (5 and 10 nm) nanoparticles to undergo extensive aggregation, which was confirmed by dynamic laser scattering measurements revealing a high polydispersity index (PDI) value of 0.54 for the 10 nm particles. This may be explained by their larger total surface-to-volume ratio, leading to incomplete PLL coverage of the particle surface. AuNPs measuring 40 nm in diameter did not show an increase in size upon PLL complexation (PDI=0.05), with a homogenous composition as seen on transmission electron microscopy (TEM) (Figure 1b). Following PLL complexation, the surface charge of naked particles changed from negatively charged (−30 to −40 mV) to positively charged (+15 to +45 mV) (Table 2).

2.2. Intracellular Labeling

Cellular uptake of AuNP-PLL-RITC complexes was assessed using brightfield microscopy, fluorescence microscopy, and TEM (Figure 2). hMSCs could be efficiently labeled when PLL was complexed to the particles, in contrast to naked citrate-stabilized AuNPs that showed almost no uptake. The AuNP-PLL-RITC complexes tended to agglomerate in the perinuclear region in a similar fashion as that seen for cells labeled with SPIO nanoparticles.^[12, 32, 34]

2.3. Functional Characterization of Labeled hMSCs

To assess whether or not the AuNP-PLL-RITC labeling interferes with cell viability and proliferation, labeled and unlabeled cells were tested with an MTS assay. The MTS assay reports on the amount of mitochondrial activity. Labeling with AuNP-PLL-RITC complexes for 12 hours did not have an adverse effect on cell viability (Figure 3). No significant difference in viability between unlabeled and labeled cells was observed ($p=0.55$). Labeled and unlabeled hMSCs were then tested for their ability to differentiate into two downstream cell lineages, i.e., adipocytes and osteocytes (Figure 4). Oil Red O staining for adipogenesis did not show any difference between labeled and unlabeled cells, with the fatty lipid deposits staining red. AuNPs were still visible at 3 weeks post labeling (Figure 4b). Similarly, von Kossa staining for osteogenesis yielded a similar black staining for calcium deposits between labeled and unlabeled cells.

2.4. In Vitro Micro-CT Imaging of Labeled hMSCs

Cells were labeled with various concentrations of AuNP-PLL-RITC complexes, washed, and suspended in 1% agarose at 1×10^6 cells per tube. As compared to agarose alone (35 HU) and unlabeled cells in agarose (45 HU), labeled cells provided a strong attenuation on micro-CT imaging (Figure 5a). Values for cells labeled with 0.025, 0.05, 0.1, and 0.2 mg Au/ml were 178, 425, 813, and 1449 HU, respectively, with a linear dependence of the attenuation on the amount of AuNP-PLL-RITC added for labeling ($r=0.99$, $p<0.05$) (Figure 5b). The intracellular Au content was determined with ICP-MS, and found to be linear with the amount of CT attenuation (Figure 5c). These results indicate that the amount of obtained CT contrast is not only proportional to the amount of internalized label,^[35] but also that the amount of particle uptake shows a linear correlation with the amount of particles added to the medium during incubation. There was no difference in the gold concentration-adjusted attenuation for internalized and cell-aggregated vs. agarose phantoms spiked with free particles, with values of 87 ($r=0.99$, $p<0.05$) and 80 ($r=0.99$, $p<0.05$) HU per mg Au ml⁻¹, respectively (Figure 5d). We then investigated the dependence of CT attenuation on cell number. Values for 3.1×10^4 , 6.3×10^4 , 1.3×10^5 , 2.5×10^5 , 5.0×10^5 , and 1.0×10^6 cells were 41, 55, 69, 143, 271, 453, and 762 HU, with an excellent linear correlation ($r=0.99$, $p<0.05$) (Figure 6). Taken together, these findings indicate that cell numbers can be quantified with CT, analogous to the use of fluorine nanoparticles in ¹⁹F MRI^[36] or magnetic nanoparticles in MPI.^[12]

2.5. In Vivo Micro-CT Imaging of Labeled hMSCs

To determine the feasibility of micro-CT imaging of AuNP-PLL-RITC-labeled hMSCs, 2×10^4 – 5×10^5 cells were transplanted in rat brain (Figure 7a). ROIs were drawn over the area of the cell transplant as well as the skull and normal brain parenchyma. From these ROIs, the HU values were calculated and are given in Table 3. Both the 5×10^5 and 2×10^5 cell transplants could be visualized, but not the transplants containing lower amounts of cells. The respective HU values were 1445, 505, 145, and 76 for 5×10^5 , 2×10^5 , 6×10^4 , and 2×10^4 cells, respectively. From these findings we conclude that the detection limit is $\sim 2 \times 10^4$ cells/ μ l for stem cell visualization by micro-CT imaging *in vivo*. It should be noted that we determined this value for the brain, and more cells may be needed in tissues that are more radio-opaque. The engraftment of AuNP-PLL-RITC-labeled cells was confirmed by immunofluorescence microscopy (Figure 7b). An excellent match of brain tissue containing dual STEM121 (human cell marker) and RITC (gold nanoparticle)-positive cells with the contrasted area on micro-CT could be observed.

One question inherent to any form of nanoparticle labeling is whether or not the signal represents live cells, which can only be answered using reporter genes. However, we anticipate CT cell tracking to have its greatest value in the immediate imaging of cell biodistribution and verification of the accuracy of cell delivery, as is the case for MRI cell tracking^[7]. In this respect, CT tracking may have a wider use, as the number of centers that can perform real-guided MRI-guided injections is very limited, in contrast to CT delivery.

3. Conclusion

In summary, 40 nm diameter AuNPs could be readily complexed with PLL in order to label hMSCs with sufficient amounts of gold to be detected on micro-CT *in vitro* and *in vivo*. The attenuated CT contrast was linear to the number of cells and the total amount of Au, was independent of the conformational state of the particles (aggregated inside cells or free in solution), and had a sensitivity threshold of approximately 2×10^4 cells/ μ l.

4. Experimental Section

Materials

AuNPs with diameters of 5, 10, 20, and 40 nm were purchased from British Biocell International (BBI, Cardiff, UK). Poly-L-lysine hydrobromide (P0879, Mw=1–5 KDa), paraformaldehyde, osmium tetroxide, Oil-red-O, rhodamine B isothiocyanate (RITC), sodium cacodylate buffer, Triton X and AAS gold standard (Catal. #08269) were purchased from Sigma-Aldrich (St. Louis, MO). Phosphate-buffered saline (PBS), fetal bovine serum (FBS), glutamax, penicillin-streptomycin, Dulbecco's Modified Eagle Medium (DMEM) and normal goat serum (NGS) (10%) were purchased from Invitrogen (Carlsbad, CA). Trypsin/ethylenediamine tetra-acetic acid (EDTA), adipogenic induction/maintenance medium, and osteogenic induction medium was purchased from Lonza (Walkersville, MD). Anti-human cytoplasmic marker antibody (STEM121) was purchased from StemCells, Inc. (Newark, CA). Goat anti-Mouse IgG H&L (FITC) was purchased from Abcam (Cambridge, MA). 100% graded ethanol, propylene oxide, lead citrate, uranyl acetate, and fluorogel in tris buffer were purchased from EM Science (Gibbstown, NJ). 4',6-diamidino-2-phenylindole (DAPI) was purchased from Roche (Indianapolis, IN). MTS ([3-(4,5-dimethylthiazol-2-yl)-5-(3-carboxymethoxyphenyl)-2-(4-sulfophenyl)-2H-tetrazolium, inner salt, Cell Titer 96[®] Aqueous, G3582) was purchased from Promega (Madison, WI).

Preparation of Au NPs-PLL (RITC) complexes

Thirty-two mL of 40 nm citrate capped AuNP solution (60 μ g Au/ml in distilled water) was mixed with 1.4 mL of PLL solution (1 mg/ml in distilled water) and stirred for 30 mins. The preparation was then centrifuged at 3,000xg for 45 mins in order to remove excess PLL, and the pellet was resuspended in 1.5 mL of distilled water. Two mg of RITC was added to the AuNP-PLL complexes to render them fluorescent, and sample tubes were stirred for 12 h protected from light. After three washing steps with distilled water by centrifugation at 3,000xg for 45 mins to remove unreacted RITC, the final AuNP-PLL-RITC solution was dispersed in 1.5 mL of distilled water.

Characterization of Au NPs-PLL(RITC) complexes

Transmission electron microscopy (TEM) analysis was conducted using a JEOL JEM-2010 transmission electron microscope operating at 200 kV. Samples were prepared by putting a drop of particle dispersion onto a carbon-coated copper grid. Dynamic light scattering (DLS) measurements were obtained to calculate the PDI using a ZEN3690 instrument (Malvern Instruments). Zeta potential measurements were obtained using a zeta-potential/particle size

analyzer (ELS-Z2, Otsuka). An inductively coupled plasma mass spectrometer (ICP-MS, ELAN 6100, Perkin-Elmer SCIEX) was used for quantitative analysis of elements.

Cell culture and cell labeling

hMSCs were cultured in DMEM supplemented with 10% FBS, 1% glutamax, and 1% penicillin-streptomycin at 37 °C in 5% CO₂ and a humidified atmosphere. Cell culture medium was changed every 2–3 days. When hMSCs reached confluence in 150 cm² flasks, they were passaged using 0.25% trypsin/EDTA, collected by centrifugation at 300xg for five mins. For all experiments, cells from passage 4–7 were used. For nanoparticle labeling, cells were grown to 80% confluence in 15 ml medium, and 1.5 mL of AuNP-PLL-RITC in PBS was added at different concentrations (0, 0.025, 0.05, 0.1, and 0.2 mg Au/ml). Cells were incubated for 12 hours and then washed with PBS 3 times. Cells were trypsinized, washed, and counted.

Microscopy

Cellular uptake was studied using bright field microscopy, fluorescence microscopy, and TEM. Labeled hMSCs were cultured in a six-well plates (Falcon #303046, non-pyrogenic). After 12 hours, cells were washed with PBS, fixed with 4% paraformaldehyde, and stained with DAPI 1 µg/ml in PBS). Fluorescence images were acquired using Olympus BX51 and IX71 epifluorescence microscopes equipped with an Olympus DP-70 digital acquisition system.

TEM images were acquired using a JEOL JEM-2010 instrument operating at 200 kV. Labeled hMSCs were cultured in six-well plates as described above, and then fixed with 4% paraformaldehyde for 2 hours. Subsequently, fixed specimens were incubated with 2% osmium tetroxide buffered in 0.1 M cacodylate buffer for 2 hours, and dehydrated with 50 to 100% graded ethanol and propylene oxide. Samples were embedded in pure Epoxy Resin at 60 °C for 3 days. Ultrathin sections were cut using glass knives and a diamond knife (Reichert-Jung, Vienna, Austria) using an ultramicrotome (RMC MTXL; Tucson, AZ, USA). Sections were stained with lead citrate and uranyl acetate before TEM analysis.

Cell viability assay

The viability and proliferation of labeled hMSCs was evaluated using an MTS assay performed in triplicate. hMSCs were seeded in triplicate into 96 well plates at a density of 5×10^3 cells per well in 200 µl of culture medium and grown overnight. AuNP-PLL-RITC complexes in PBS were added at different concentrations (0, 0.025, 0.05, 0.1, and 0.2 mg Au/ml). After 12h incubation, cells were washed with PBS. 20 µl of Cell Titer 96[®] Aqueous One Solution Reagent and 100 µl culture medium was added to each well. Cells were incubated for 2 hours at 37 °C in a humidified 5% CO₂ atmosphere. The absorbance was then recorded at 490 nm using a 96-well micro plate reader (Victor3, Perkin Elmer, Waltham, MA).

In vitro cell differentiation studies

Labeled (0.05 mg Au/ml) and unlabeled (control) hMSCs were induced to differentiate into the adipogenic and osteogenic lineages. After cells were grown confluent in 6-well plates,

the growth medium was replaced with adipogenic induction medium (DMEM, 10% fetal bovine serum, 1% penicillin-streptomycin, 1% glutamax, 1 μ M dexamethasone, 10 μ g/ml 3-isobutyl-1-methylxanthine, 10 μ g/ml insulin, and 100 μ M indomethacin, Lonza). After three days, the adipogenic induction medium was replaced with adipogenic maintenance medium for one day (DMEM, 10% fetal bovine serum, 1% penicillin-streptomycin, 1% glutamax, and 10 μ g/ml insulin, Lonza). Three cycles of induction and maintenance were performed, after which the cells were incubated in adipogenic maintenance medium for seven days. Control cells were supplemented only with adipogenic maintenance medium. Oil Red O staining was used to assess adipogenesis. To this end, cells were fixed in 10% formalin and then incubated in 60% isopropanol for four mins. The cells were then incubated in Oil Red O staining solution for five mins, rinsed in distilled water, and counterstained in hematoxylin for one min. After washing with distilled water, slides were mounted and examined using Olympus BX51 and IX71 epifluorescence microscopes equipped with an Olympus DP-70 digital acquisition system.

Osteogenesis was initiated when hMSCs were confluent. The medium was replaced with osteogenic induction medium (DMEM, 10% fetal bovine serum, 1% penicillin-streptomycin, 1% glutamax, 50 μ g/ml ascorbic acid, 100 nM dexamethasone, and 10 mM beta-glycerophosphate disodium salt hydrate, Lonza). Osteogenesis was induced over a period of two weeks, and a von Kossa staining kit (Fisher Sci., Waltham, MA) was used to assess osteogenesis. To this end, cells were fixed in 10% formalin and then incubated in 5% silver nitrate for 40 mins with exposure to ultraviolet light. Cells were washed in distilled water and then placed in 5% sodium thiosulfate for two mins, after which they were rinsed in distilled water and incubated with nuclear fast red stain for five mins. After washing with distilled water, slides were mounted and viewed using Olympus BX51 and IX71 epifluorescence microscopes equipped with an Olympus DP-70 digital acquisition system.

Micro-CT imaging of labeled cells in vitro

For *in vitro* phantom preparations, 1×10^6 cells labeled with different concentrations of AuNP-PLL-RITC complexes were suspended in 25 μ l of PBS in 0.1 mL polymerase chain reaction (PCR, Thermo Fisher Sci.) tubes and mixed with 25 μ l of 2% agarose in PBS. The final concentration was 2×10^4 cells/ μ l in 1% agarose. Different numbers of labeled cells (1×10^6 , 5×10^5 , 2.5×10^5 , 1.3×10^5 , 6.3×10^4 , and 3.1×10^4 cells) were suspended in 25 μ l of PBS in 0.1 mL PCR tubes and mixed with 25 μ l of 2% agarose in PBS. The final cell concentrations were 2×10^4 , 1×10^4 , 5×10^3 , 2.5×10^3 , 1.3×10^3 , and 6.2×10^2 cells/ μ l in 1% agarose, respectively.

In vitro micro-CT imaging of the cell suspensions was performed using a X-SPECT Gamma Medica imager (Gamma Medica-Ideas, Northridge, CA) with tube settings of 75.16 kV and 240.3 mA, a 64-mm detector setting, and 512 projections obtained at 1° for a full 360° rotation. Scanning was performed in a clockwise direction with an X-ray tube-to-detector distance of 269 mm and an X-ray tube-to-center of rotation distance of 225 mm. Images were reconstructed into axial sections with 512×512 pixels per section using standard back projection techniques. Images were processed using ImageJ.

Measurement of intracellular gold content

After imaging, the cell suspension samples were assayed for gold content using ICP-MS analysis (ELAN 6100; Perkin-Elmer SCIEX). A standard curve was used to quantify the amount of intracellular gold. Briefly, standard solutions were made by diluting the AAS gold standard in the PBS/agarose mixture used for the cell suspensions. The intracellular gold concentration was calculated by dividing the total gold content by the number of cells or agarose volume.

Micro-CT imaging of labeled cells in vivo

All animal experiments were approved by our Institutional Animal Care and Use Committee. Male Sprague Dawley rats (350 g) were anesthetized with 1–2% isoflurane, and positioned in a stereotaxic device (Stoelting, Wood Dale, IL, USA). A small skin incision was made in the midline to expose the skull. Cells were labeled for 12 hours with 0.1 mg Au/ml. Using a motorized nanoinjector (Stoelting, Inc.) and a Hamilton syringe (Hamilton, Reno, NV) attached to a 33 G needle, 10 μ l of sterile PBS containing 5.0×10^5 , 2×10^5 , 6×10^4 , or 2×10^4 labeled cells, or unlabeled hMSCs, was injected into the striatum according to the following coordinates from bregma: anteroposterior [AP] = 0.0 mm; mediolateral [ML] = –3.0/3.0 mm; and dorsoventral [DV] = –5.0 mm. Cells were injected slowly over 10 min, and the needle was left in place for 1 min before being withdrawn. The incision was closed, and postoperative analgesia was provided with Ketofen. Micro-CT imaging was performed at 30 mins post-injection using the same X-SPECT Gamma Medica imager with tube settings of 75.16 kV and 240.3 mA, a 64-mm detector setting, and 512 projections obtained at 1° for a full 360° rotation.

Hounsfield Unit (HU) measurements

To quantify CT signal intensity as Hounsfield Units (HU), a two-point calibration method was used. The CT signal intensity in water was set to 0 HU, and that for ambient air to –1,000 HU. Sample HU values were then obtained by linear extrapolation using

$$HU = 1000 \times \frac{\mu_x - \mu_{water}}{\mu_{water} - \mu_{air}}$$

where, μ_x , μ_{water} , and μ_{air} are the linear attenuation coefficients of the sample, water, and air, respectively.

Immunostaining

After imaging, animals were euthanized and perfused with 4% paraformaldehyde (PFA). Tissues were cryoprotected in sucrose and cut with a Microm HM 505 E Cryostat. After fixation with 4% PFA for 10 min, tissue sections were dried for 1 h at 50 °C. After washing 3 times with PBS, tissues were incubated with 0.1% Triton X and 10% normal goat serum (NGS) blocking solution for 1 hour, and then incubated with primary mouse anti-human cytoplasmic marker antibody (STEM12, 1:1000 diluted in PBS) for 24 h. After washing 2 times with PBS, a goat anti-mouse FITC conjugated secondary antibody was added (ab6785, 1:300 diluted in PBS) for 1 hour. After washing 2 times with PBS, slides were mounted with

fluorogel in tris buffer (EMS catal# 17985-10) and examined with Olympus BX51 and IX71 epifluorescence microscopes equipped with an Olympus DP-70 digital acquisition system. Negative controls consisted of omission of the primary antibody.

Statistical analysis

All statistical calculations were performed using SAS 9.4. A type III test of fixed effects embedded within PROC MIXED was used to determine statistical significance. The lowest mean square difference test was employed for comparison between means. The Pearson correlation coefficient embedded within PROC CORR was used to determine statistical relationship between variables, with a threshold of $p=0.05$.

Acknowledgments

This work was supported by NIH 2R01 NS045062, the Maryland Nanotechnology Research and Industry Fund, the Global Research Lab program funded by the National Research Foundation of Korea, and the Research Center Program of Institute for Basic Science (IBS) in Korea.

References

1. Carpenter MK, Frey-Vasconcells J, Rao MS. *Nat Biotechnol.* 2009; 27:606. [PubMed: 19587662]
Zimmermann WH, Melnychenko I, Wasmeier G, Didie M, Naito H, Nixdorff U, Hess A, Budinsky L, Brune K, Michaelis B, Dhein S, Schwoerer A, Ehmke H, Eschenhagen T. *Nature medicine.* 2006; 12:452.
2. Petite H, Viateau V, Bensaid W, Meunier A, de Pollak C, Bourguignon M, Oudina K, Sedel L, Guillemain G. *Nat Biotechnol.* 2000; 18:959. [PubMed: 10973216]
3. Wakitani S, Goto T, Pineda SJ, Young RG, Mansour JM, Caplan AI, Goldberg VM. *J Bone Joint Surg-Am Vol.* 1994; 76A:579.
4. Badorff C. *Circulation.* 2003; 107:1024. [PubMed: 12600917]
5. Hunsberger JG, Rao M, Kurtzberg J, Bulte JW, Atala A, LaFerla FM, Greely HT, Sawa A, Gandy S, Schneider LS, Doraiswamy PM. *Lancet Neurol.* 2015
6. Liechty KW, MacKenzie TC, Shaaban AF, Radu A, Moseley AB, Deans R, Marshak DR, Flake AW. *Nature medicine.* 2000; 6:1282. Pittenger MF. *Science.* 1999; 284:143. [PubMed: 10102814]
7. Bulte JW. *AJR Am J Roentgenol.* 2009; 193:314. [PubMed: 19620426]
8. Naumova AV, Modo M, Moore A, Murry CE, Frank JA. *Nat Biotechnol.* 2014; 32:804. [PubMed: 25093889]
9. Yaghoubi SS, Jensen MC, Satyamurthy N, Budhiraja S, Paik D, Czernin J, Gambhir SS. *Nat Clin Pract Oncol.* 2009; 6:53. [PubMed: 19015650]
10. Chin BB, Nakamoto Y, Bulte JW, Pittenger MF, Wahl R, Kraitchman DL. *Nucl Med Commun.* 2003; 24:1149. [PubMed: 14569169]
11. Ahrens ET, Bulte JW. *Nat Rev Immunol.* 2013; 13:755. [PubMed: 24013185]
12. Bulte JW, Walczak P, Janowski M, Krishnan KM, Arami H, Halkola A, Gleich B, Rahmer J. *Tomography.* 2015; 1:91. [PubMed: 26740972]
13. Zheng B, Vazin T, Goodwill PW, Conway A, Verma A, Saritas EU, Schaffer D, Conolly SM. *Sci Rep.* 2015; 5:14055. [PubMed: 26358296]
14. Jokerst JV, Khademi C, Gambhir SS. *Sci Transl Med.* 2013; 5:177ra35. Cui W, Tavri S, Benchimol MJ, Itani M, Olson ES, Zhang H, Decyk M, Ramirez RG, Barback CV, Kono Y, Mattrey RF. *Biomaterials.* 2013; 34:4926. [PubMed: 23578557]
15. Schwenzer NF, Springer F, Schraml C, Stefan N, Machann J, Schick F. *Journal of hepatology.* 2009; 51:433. [PubMed: 19604596] Lee N, Choi SH, Hyeon T. *Advanced materials.* 2013; 25:2641. [PubMed: 23553799] Liu YL, Ai KL, Lu LH. *Accounts Chem Res.* 2012; 45:1817.

16. Shilo M, Reuveni T, Motiei M, Popovtzer R. *Nanomedicine*. 2012; 7:257. [PubMed: 22339135] Cormode DP, Naha PC, Fayad ZA. *Contrast media & molecular imaging*. 2014; 9:37. [PubMed: 24470293] Pan D, Lanza GM, Wickline SA, Caruthers SD. *European journal of radiology*. 2009; 70:274. [PubMed: 19268515]
17. Rabin O, Manuel Perez J, Grimm J, Wojtkiewicz G, Weissleder R. *Nature materials*. 2006; 5:118. [PubMed: 16444262] Brown AL, Naha PC, Benavides-Montes V, Litt HI, Goforth AM, Cormode DP. *Chemistry of materials : a publication of the American Chemical Society*. 2014; 26:2266. [PubMed: 24803727]
18. Liu Y, Ai K, Liu J, Yuan Q, He Y, Lu L. *Angewandte Chemie*. 2012; 51:1437. [PubMed: 22223303] Pan DPJ, Schirra CO, Senpan A, Schmieder AH, Stacy AJ, Roessl E, Thran A, Wickline SA, Proska R, Lanza GM. *ACS Nano*. 2012; 6:3364. [PubMed: 22385324]
19. Jakhmola A, Anton N, Anton H, Messaddeq N, Hallouard F, Klymchenko A, Mely Y, Vandamme TF. *Biomaterials*. 2014; 35:2981. [PubMed: 24393266]
20. Oh MH, Lee N, Kim H, Park SP, Piao Y, Lee J, Jun SW, Moon WK, Choi SH, Hyeon T. *Journal of the American Chemical Society*. 2011; 133:5508. [PubMed: 21428437] Bonitatibus PJ Jr, Torres AS, Goddard GD, FitzGerald PF, Kulkarni AM. *Chemical communications*. 2010; 46:8956. [PubMed: 20976321]
21. Dekrafft KE, Boyle WS, Burk LM, Zhou OZ, Lin W. *J Mater Chem*. 2012; 22:18139. [PubMed: 23049169]
22. Popovtzer R, Agrawal A, Kotov NA, Popovtzer A, Balter J, Carey TE, Kopelman R. *Nano Lett*. 2008; 8:4593. [PubMed: 19367807] Kim D, Park S, Lee JH, Jeong YY, Jon S. *Journal of the American Chemical Society*. 2007; 129:7661. [PubMed: 17530850] Wang H, Zheng L, Peng C, Guo R, Shen M, Shi X, Zhang G. *Biomaterials*. 2011; 32:2979. [PubMed: 21277019] Hainfeld JF, Slatkin DN, Focella TM, Smilowitz HM. *The British journal of radiology*. 2006; 79:248. [PubMed: 16498039] Sun IC, Eun DK, Na JH, Lee S, Kim IJ, Youn IC, Ko CY, Kim HS, Lim D, Choi K, Messersmith PB, Park TG, Kim SY, Kwon IC, Kim K, Ahn CH. *Chemistry*. 2009; 15:13341. [PubMed: 19902441] Xi D, Dong S, Meng X, Lu Q, Meng L, Ye J. *RSC Advances*. 2012; 2:12515.
23. Jackson PA, Rahman WN, Wong CJ, Ackerly T, Geso M. *European journal of radiology*. 2010; 75:104. [PubMed: 19406594]
24. Xu CJ, Tung GA, Sun SH. *Chem Mat*. 2008; 20:4167.
25. Alkilany AM, Murphy CJ. *Journal of nanoparticle research : an interdisciplinary forum for nanoscale science and technology*. 2010; 12:2313. [PubMed: 21170131] Connor EE, Mwamuka J, Gole A, Murphy CJ, Wyatt MD. *Small*. 2005; 1:325. [PubMed: 17193451] Ricles LM, Nam SY, Sokolov K, Emelianov SY, Suggs LJ. *International Journal of Nanomedicine*. 2011; 6:407. [PubMed: 21499430]
26. Cormode DP, Roessl E, Thran A, Skajaa T, Gordon RE, Schlomka JP, Fuster V, Fisher EA, Mulder WJ, Proksa R, Fayad ZA. *Radiology*. 2010; 256:774. [PubMed: 20668118] Mieszawska AJ, Mulder WJ, Fayad ZA, Cormode DP. *Mol Pharm*. 2013; 10:831. [PubMed: 23360440]
27. Arifin DR, Long CM, Gilad AA, Alric CE, Roux S, Tillement O, Link TW, Arepally A, Bulte JWM. *Radiology*. 2011; 260:790. [PubMed: 21734156] Kim J, Arifin DR, Muja N, Kim T, Gilad AA, Kim H, Arepally A, Hyeon T, Bulte JW. *Angewandte Chemie*. 2011; 50:2317. [PubMed: 21351344]
28. Chhour P, Naha PC, O'Neill SM, Litt HI, Reilly MP, Ferrari VA, Cormode DP. *Biomaterials*. 2016; 87:93. [PubMed: 26914700]
29. Meir R, Shamalov K, Betzer O, Motiei M, Horovitz-Fried M, Yehuda R, Popovtzer A, Popovtzer R, Cohen CJ. *ACS Nano*. 2015; 9:6363. [PubMed: 26039633]
30. Zhdanov RI, Podobed OV, Vlassov VV. *Bioelectrochemistry*. 2002; 58:53. [PubMed: 12401571]
31. Kalish H, Arbab AS, Miller BR, Lewis BK, Zywicke HA, Bulte JW, Bryant LH Jr, Frank JA. *Magnetic resonance in medicine*. 2003; 50:275. [PubMed: 12876703]
32. Frank JA, Miller BR, Arbab AS, Zywicke HA, Jordan EK, Lewis BK, Bryant LH, Bulte JWM. *Radiology*. 2003; 228:480. [PubMed: 12819345]
33. Zhou D, Li C, Hu Y, Zhou H, Chen J, Zhang Z, Guo T. *Journal of Materials Chemistry*. 2012; 22:10743.

34. Kim HS, Oh SY, Joo HJ, Son KR, Song IC, Moon WK. NMR in biomedicine. 2010; 23:514. [PubMed: 20175151]
35. Galper MW, Saung MT, Fuster V, Roessl E, Thran A, Proksa R, Fayad ZA, Cormode DP. Invest Radiol. 2012; 47:475. [PubMed: 22766909]
36. Srinivas M, Morel PA, Ernst LA, Laidlaw DH, Ahrens ET. Magnetic resonance in medicine. 2007; 58:725. [PubMed: 17899609]

Author Manuscript

Author Manuscript

Author Manuscript

Author Manuscript

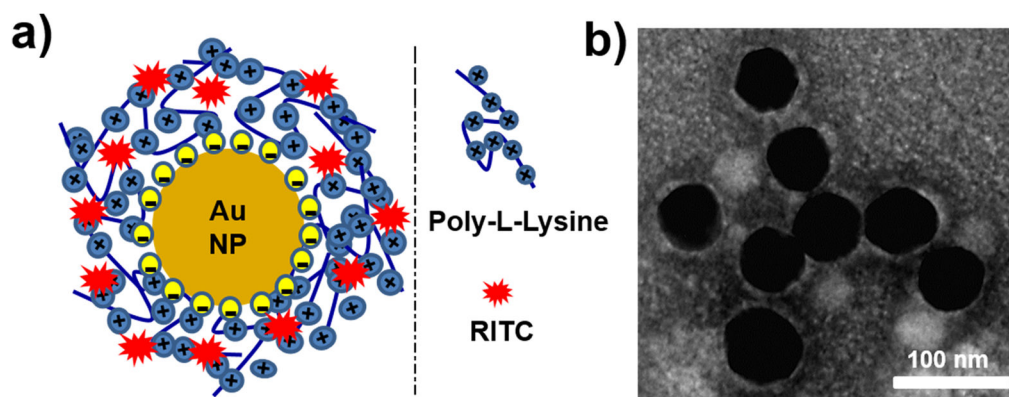


Figure 1. (a) Schematic illustration and (b) TEM of 40 nm core diameter AuNP-PLL-RITC-complexes.

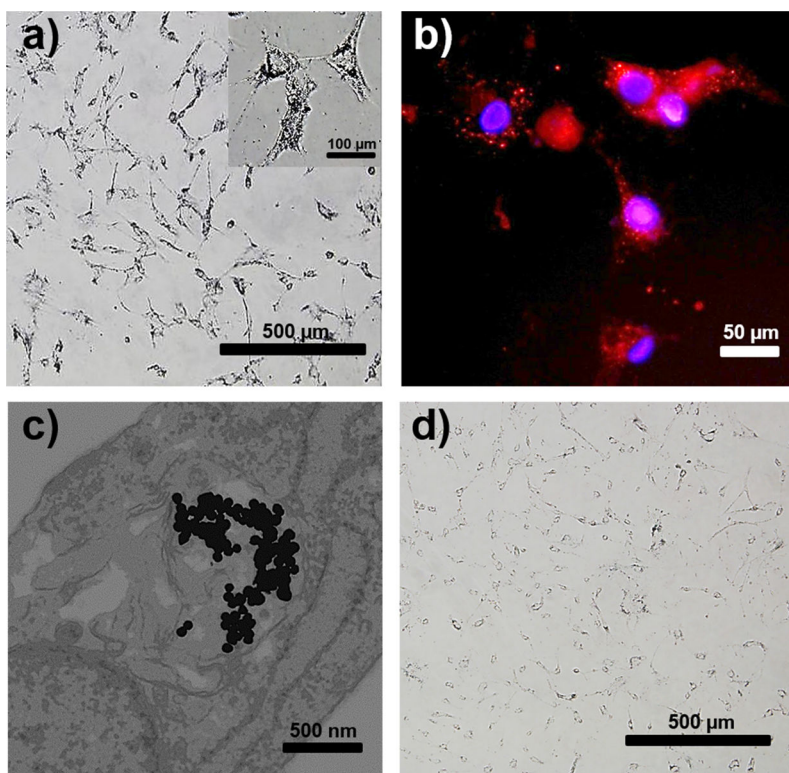


Figure 2. Intracellular uptake of AuNP-PLL-RITC in hMSCs. Shown are (a) brightfield, (b) fluorescence (blue=DAPI, red=RITC), and (c) TEM images. The intracellular uptake of uncomplexed (naked) citrate AuNPs is negligible, as shown in (d).

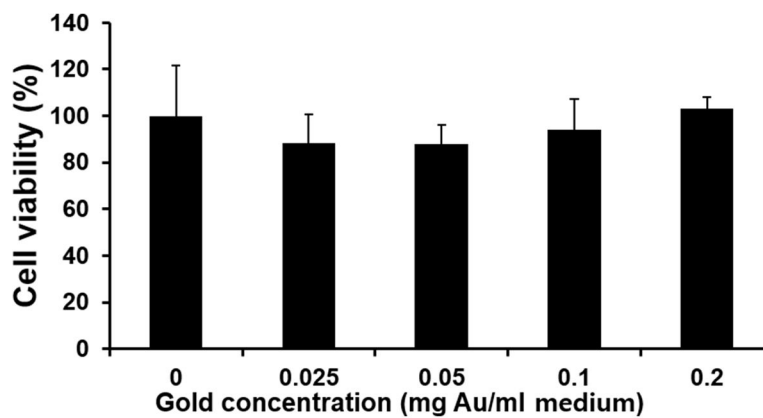


Figure 3. Assessment of cell viability and proliferation using an MTS assay for varying AuNP-PLL-RITC concentrations. Cells were incubated for 1 day at 37 °C.

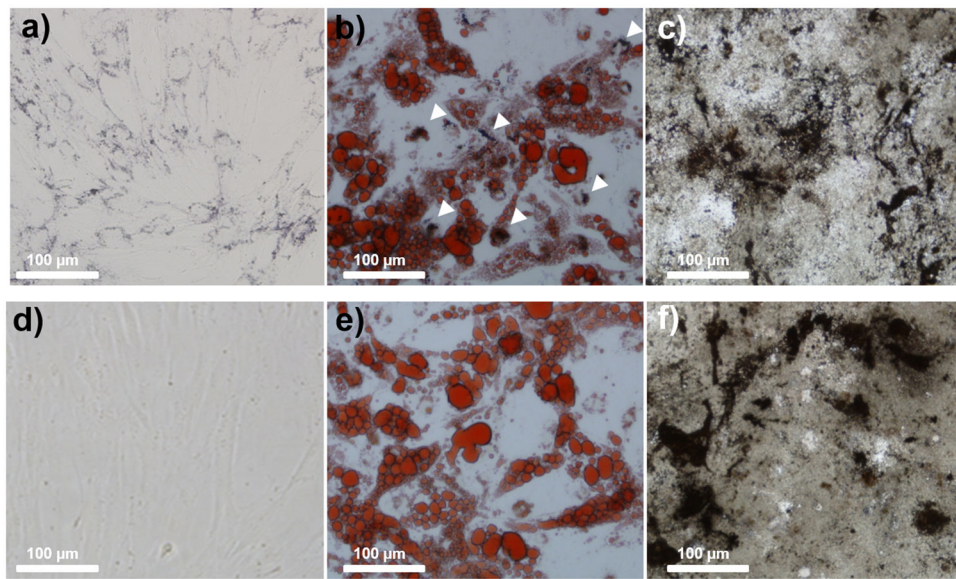


Figure 4. Differentiation of AuNP-PLL-RITC labeled (a–c) and unlabeled (d–f) hMSCs. Images were taken 3 weeks post-labeling. Shown are unstained images (a,d), Oil Red O staining for adipocytes (b,e), and von Kossa staining for osteocytes (c,f). Arrows in (b) indicate the retention of AuNP-PLL-RITC nanoparticles.

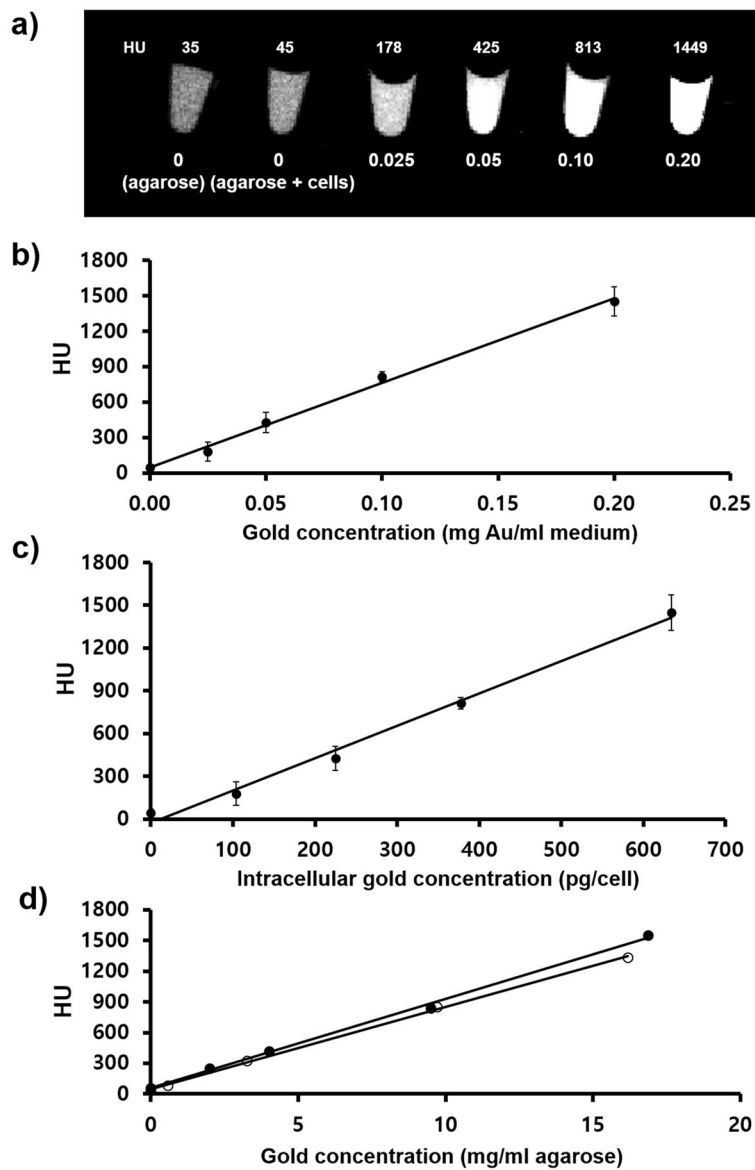


Figure 5.

(a) *In vitro* micro-CT imaging of agarose phantoms containing 1×10^6 hMSCs labeled with different concentrations of AuNP-PLL-RITC complexes, given as mg Au/ml. (b) Calculated HU values show a linear dependence with the concentration of AuNP-PLL used for cell labeling ($r=0.99$, $p<0.05$). (c) Calculated HU values show a linear dependence with the intracellular Au concentration as determined by ICP-MS ($r=0.99$, $p<0.05$) (d) HU value comparison shows no significant difference in attenuation between intracellular (○) versus non-cell bound (free, ●) AuNP-PLL-RITC complexes.

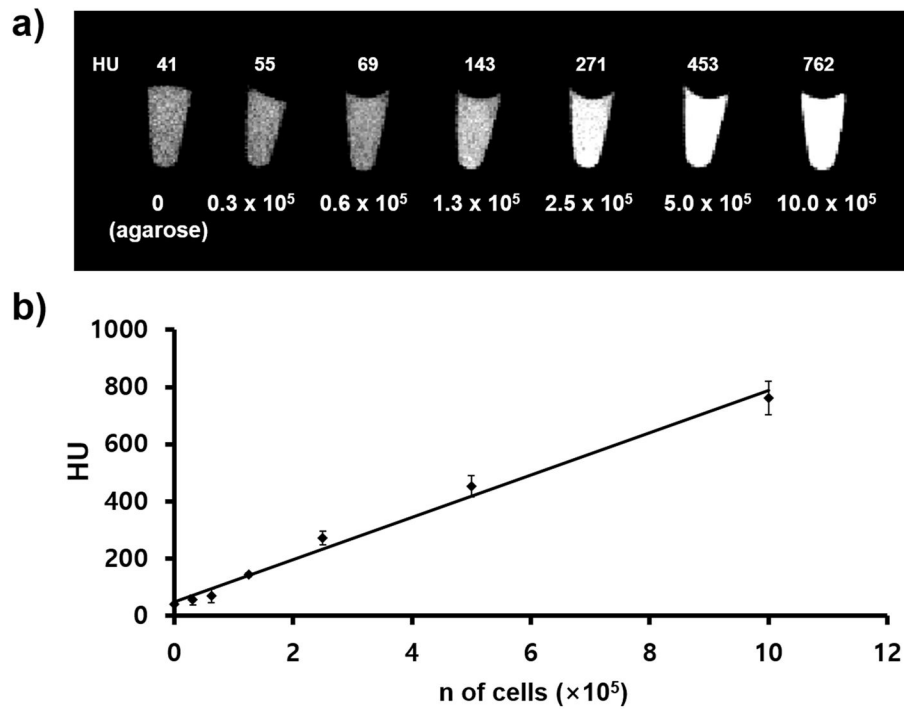


Figure 6.

(a) *In vitro* micro-CT imaging of agarose phantoms containing different amounts of hMSCs labeled 0.1 mg Au/ml AuNP-PLL-RITC complexes. (b) Calculated HU values show a linear concentration with the number of cells ($r=0.99$).

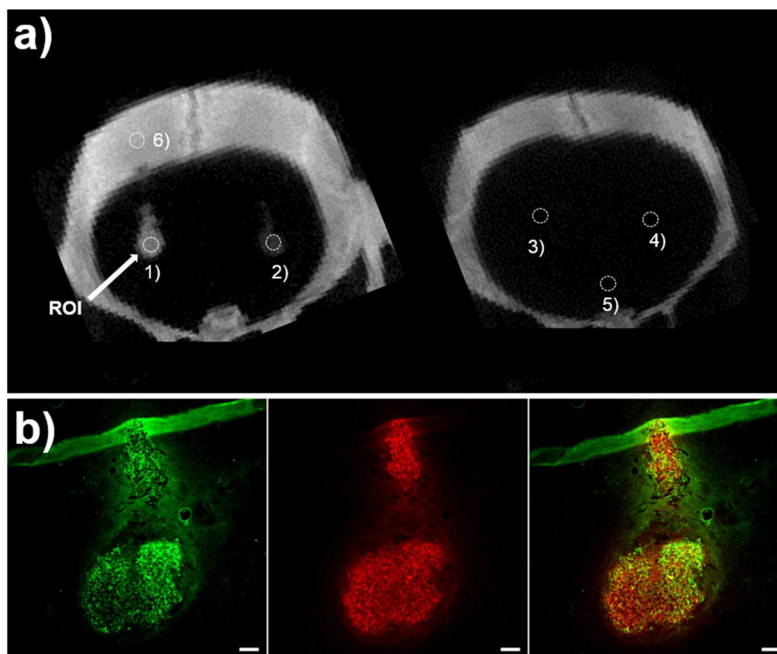


Figure 7.

(a) *In vivo* micro-CT images of AuNP-PLL-RITC-labeled hMSCs at 30 min after transplantation into the striatum. The number of transplanted cells was 1) 5×10^5 cells; 2) 2×10^5 cells; 3) 6×10^4 cells; and 4) 2×10^4 cells. (b) Immunofluorescence microscopic images of the corresponding brain tissue section for injection 1) in panel a). Left: Transplanted hMSCs stained with anti-human cytoplasmic (STEM121) antibody (green). Middle: Labeling with AuNPs-PLL-RITC-complexes (red). Right: Merged image. Scale bar = 200 μm .

Table 1

Measured hydrodynamic diameter of naked AuNP particles and AuNP-PLL-RITC complexes. The left column represents the diameter as provided by the manufacturer.

Diameter	AuNP	AuNP-PLL-RITC
5 nm	6.99 ± 0.35 nm	680.97 ± 50.64 nm
10 nm	9.05 ± 0.07 nm	198.23 ± 62.66 nm
20 nm	18.93 ± 0.91 nm	70.89 ± 19.97 nm
40 nm	38.24 ± 0.99 nm	43.78 ± 7.81 nm

Author Manuscript

Author Manuscript

Author Manuscript

Author Manuscript

Table 2

Measured electrophoretic (zeta) potential (ζ) of naked AuNP particles and AuNP-PLL-RITC complexes. The left column represents the diameter as provided by the manufacturer.

Diameter	AuNP	AuNP-PLL-RITC
5 nm	-41.85 ± 13.93 mV	$+15.40 \pm 0.41$ mV
10 nm	-37.95 ± 1.91 mV	$+20.45 \pm 1.06$ mV
20 nm	-40.60 ± 0.99 mV	$+21.95 \pm 0.92$ mV
40 nm	-39.80 ± 0.42 mV	$+48.35 \pm 0.35$ mV

Author Manuscript

Author Manuscript

Author Manuscript

Author Manuscript

Table 3

HU measurements from the corresponding ROIs shown in Figure 7.

ROI	Description	HU value
1	5×10^5 cells	1445
2	2×10^5 cells	505
3	6×10^4 cells	145
4	2×10^4 cells	76
5	Brain parenchyma	60
6	Skull	2340

Author Manuscript

Author Manuscript

Author Manuscript

Author Manuscript